

A STUDY OF THE SHADOWING OF GALACTIC COSMIC RAYS BY THE SUN IN A QUIET PHASE OF SOLAR ACTIVITY WITH THE TIBET AIR SHOWER ARRAY

M. Amenomori¹, S. Ayabe², Caidong³, Danzengluobu³, L.K. Ding⁴, Z.Y. Feng⁵, Y. Fu⁶, H.W. Guo³, M. He⁶, K. Hibino⁷, N. Hotta⁸, Q. Huang⁵, A.X. Huo⁴, K. Izu⁹, H.Y. Jia⁵, F. Kajino¹⁰, K. Kasahara¹¹, Y. Katayose¹², Labaciren³, J.Y. Li⁶, H. Lu⁴, S.L. Lu⁴, G.X. Luo⁴, X.R. Meng³, K. Mizutani², J. Mu¹³, H. Nanjo¹, M. Nishizawa¹⁴, M. Ohnishi⁹, I. Ohta⁸, T. Ouchi⁷, Z.R. Peng⁴, J.R. Ren⁴, T. Saito¹⁵, M. Sakata¹⁰, T. Sasaki¹⁰, Z.Z. Shi⁴, M. Shibata¹², A. Shiomi⁹, T. Shirai⁷, Y. Suga¹⁰, H. Sugimoto¹⁶, K. Taira¹⁶, Y.H. Tan⁴, N. Tateyama⁷, S. Torii⁷, T. Utsugi², C.R. Wang⁶, H. Wang⁴, X.W. Xu^{4,9}, Y. Yamamoto¹⁰, G.C. Yu³, A.F. Yuan³, T. Yuda^{9,17}, C.S. Zhang⁴, H.M. Zhang⁴, J.L. Zhang⁴, N.J. Zhang⁶, X.Y. Zhang⁶, Zhaxiciren³, and Zhaxisangzhu³
(The Tibet AS γ Collaboration)

¹ Department of Physics, Hirosaki University, Hirosaki 036-8561, Japan

² Department of Physics, Saitama University, Urawa 338-8570, Japan

³ Department of Mathematics and Physics, Tibet University, Lhasa 850000, China

⁴ Laboratory of Cosmic Ray and High Energy Astrophysics, Institute of High Energy Physics, Academia Sinica, Beijing 100039, China

⁵ Department of Physics, South West Jiaotong University, Chengdu 610031, China

⁶ Department of Physics, Shangdong University, Jinan 250100, China

⁷ Faculty of Engineering, Kanagawa University, Yokohama 221-8686, Japan

⁸ Faculty of Education, Utsunomiya University, Utsunomiya 321-8505, Japan

⁹ Institute for Cosmic Ray Research, University of Tokyo, Kashiwa 277-8582, Japan

¹⁰ Department of Physics, Konan University, Kobe 658-8501, Japan

¹¹ Faculty of Systems Engineering, Shibaura Institute of Technology, Omiya 330-8570, Japan

¹² Faculty of Engineering, Yokohama National University, Yokohama 240-0067, Japan

¹³ Department of Physics, Yunnan University, Kunming 650091, China

¹⁴ National Institute of Information and Communications Technology, Tokyo 101-8430, Japan

¹⁵ Tokyo Metropolitan College of Aeronautical Engineering, Tokyo 116-0003, Japan

¹⁶ Shonan Institute of Technology, Fujisawa 251-8511, Japan

¹⁷ Solar-Terrestrial Environment Laboratory, Nagoya University, Nagoya 464-8601, Japan

ABSTRACT

We have shown that the Sun’s shadow by high energy cosmic rays moves year by year and its behavior is correlated with a time variation of the large-scale structure of the solar and interplanetary magnetic fields. The solar activity was near minimum in the period from 1996 through 1997. Using the data obtained with the Tibet air shower array, we examined the shadowing of cosmic rays by the Sun in this quiet phase of solar cycle, and found that the Sun’s shadow was just in the apparent direction of the Sun, though it was observed at the position considerably away from the Sun to the south-west in the period between 1990 and 1993. It is known that the magnetic pole of equivalent solar dipole was reversed during the previous active phase, and near solar minimum the dipole was aligned with the rotating axis, preserving its N-pole on the north pole side of the Sun. This causes the solar magnetic field to shift the Sun’s shadow to the east. Thus, the observed results suggest that the shift of the Sun’s shadow due to the solar magnetic field was pushed back by the effect of the geomagnetic field, since the geomagnetic field always make the shadow shift to the west. We discuss the Sun’s shadow observed during the period near solar minimum in 1996-1997 and compare it with the simulation results.

Subject headings: cosmic rays : observations — interplanetary medium — magnetic fields — solar-terrestrial relations — solar wind

1. INTRODUCTION

The Sun casts the shadow in the galactic cosmic-ray flux coming from the direction of the Sun. As almost all cosmic rays are positively charged particles, they are somewhat bent by the magnetic fields between the Sun and the Earth if their energies are not so high and eventually this effect will make the Sun’s shadow shift to a position away from the apparent Sun’s direction. This effect was first observed with the Tibet-I air shower array, operating at Yangbajing in Tibet (4,300m above sea level) since 1990, in 1993 (Amenomori et al. 1993a). We have also shown that the displacement of the Sun’s shadow is strongly correlated with the cycle of solar activity (Amenomori et al. 1993b ; Amenomori et al. 1996).

It is known that the interplanetary magnetic field (IMF) is formed as a result of the transport of the photospheric magnetic field by the solar wind flowing continuously from

the Sun (Parker 1963). Field lines near the solar equator form closed loops (neutral sheet), while field lines from the poles are dragged far into interplanetary space by the high speed solar wind of about 800 km/s. Furthermore, the magnetic field of the Sun changes sign from south to north across the neutral sheet. Accordingly the IMF is organized into large regions of opposite polarity separated by the neutral sheet, which is wavy and is inclined to the plane of the ecliptic. Then, the large-scale structure of the warped neutral sheet causes a sector structure of the IMF with the field direction reversing across the sector boundary (Wilcox & Ness 1965) so that the magnetic field points inward in some sectors and outward in others. This sector structure (“toward” and “away”) observed in the IMF, however, would vary with the phase of the solar activity cycle. The existence of the neutral sheet has been well-established observationally since the work by Smith et al. (Smith et al. 1978).

The IMF structure can be explained fairly well by the so-called “ballerina skirt” model assuming a rotating dipole in the Sun (Schultz 1973 ; Saito 1975 ; Svalgaard & Wilcox 1978), though direct evidence for the presence of such rotating dipole has not been obtained yet. In this model the variations and the reversal of the polar fields are characterized in terms of the rotating dipole. Near solar minimum the dipole is aligned with the rotating axis. Rotating slowly, the dipole becomes equatorial near maximum and finally approaches the rotation axis again near the following minimum, but pointing in the opposite direction. This model also predicts a planar neutral sheet with relatively small warps near solar minimum.

The *Ulysses* mission explored the magnetic field of the Sun’s south polar region at the radial distance of about 2.3 AU from the Sun being at near solar minimum activity (Smith et al. 1995 ; Fisk 1997). The radial component of the magnetic field is most easily related to the global solar magnetic field. If the solar magnetic field is of dipolar form, its magnitude is expected to vary with latitude and the field strength should show a significant increase over the polar region. Actually many models of the solar magnetic field discussed in the past had assumed a field similar to that of a dipole. *Ulysses*, however, found that the radial component of the magnetic field was independent of latitude (Smith & Balogh 1995 ; Balogh et al. 1995), that is, the dipolar pattern of the field strength is not reflected in the heliospheric magnetic field. It is known that the magnetic field in the high speed solar wind originates in the polar coronal hole occupying a limited region near the pole of the Sun. Then, the *Ulysses* data may suggest that a dipolar pattern close to the surface of the Sun becomes a uniform pattern at the location where the solar wind begins to flow radially outward.

Fisk discussed a model to interpret the *Ulysses* data (Fisk 1996). This model assumes that the magnetic field in the inner corona of the polar coronal hole can be represented by a tilted dipole, which has a magnetic axis offset from the solar rotation axis, and which rotates

rigidly at the equatorial rotation speed. The field lines are anchored in the photosphere, which differentially rotates, while corona holes rotate rigidly at near the equatorial rotation rate. Then a field line will move through the corona hole pattern and experience a variety of non-radial expansion in the corona hole. As the field lines open into the heliosphere, they expand in heliomagnetic latitude so that the magnetic field strength that is dipolar near the solar surface becomes uniform in the heliosphere.

In any case, as discussed above, the dipolar field of the Sun plays a major role for the origin of the IMF structure. In the previous papers (Amenomori et al. 1993b ; Amenomori et al. 1996), we showed that the Sun’s shadow is sensitive to the magnetic field close to the Sun (< 10 times the solar radius), where any spacecraft mission can not approach. Hence the continuous observation of the Sun’s shadow over the cycle of solar activity may reveal a great deal about the behavior of a rotating dipole in the Sun, if it is in existence.

When the Sun is in a quiet phase, the solar magnetic field is symmetric between the northern and southern hemisphere of the Sun. Certainly *Ulysses* in 1994 observed nearly the same magnetic field in both hemispheres. With increasing solar activity, however, the number and the activity of solar active regions tend to increase and these active regions disturb the configuration of the solar magnetic field. This effect should be reflected on the Sun’s shadow. Actually, the Sun’s shadow was observed in the direction shifted considerably from the Sun’s direction to the south-westward in 1990-1993 (Amenomori et al. 1993a ; Amenomori et al. 1996). This period was just in the active phase of solar cycle, so the observed displacement can be attributed to a change of the solar magnetic field. The solar activity, however, was near minimum in 1996-1997. During this period, then, we may be able to observe a direct effect of the equivalent solar dipole field on the Sun’s shadow. We examine this for the first time in this paper.

2. EXPERIMENT

The Tibet-I air shower array (Amenomori et al. 1992) was updated by increasing the number of counters in 1995. Since then this new air shower array (Tibet-II) has been successfully operated. The Tibet-II array, consisting of 221 scintillation counters each being placed on a lattice of 15 m spacing with a covering area of 36,900 m², has been triggering the air shower events at a rate of about 200 Hz under any 4-fold coincidence in the detectors. Its effective area is about 7 times as large as the Tibet-I array.

We analyzed the data set taken during the period from 1995 October through 1997 August. The event selection was made as in our previous analysis (Amenomori et al.

1993a). For the analysis of the shadows of the Moon and the Sun, we further selected the events within a circle of the radius 8° of the Moon and the Sun with the zenith angle less than 45° . A coordinate system was fixed on the object, putting the origin of coordinates on its center. The position of each event observed is then specified by the angular distance θ and the position angle ϕ , where θ and ϕ are measured from the center and from the north direction, respectively. In the following, we chose the equatorial coordinates for the Moon and the ecliptic coordinates for the Sun, respectively. The event distributions plotted in such coordinate systems are used to examine the shadowing of cosmic rays by these objects (Amenomori et al. 1993a).

In this paper, our analysis is focused on the Sun’s shadow observed with the Tibet II array during the period from 1995 through 1997, which almost corresponds to near minimum of the cycle of solar activity changing with a 11 year period. The Ulysses result (Fisk 1997) shows that during the current cycle the polarity is outward in the northern hemisphere and inward in the southern hemisphere, that is, N-pole of the solar dipole is in the northern hemisphere.

3. MOON’S SHADOW AND GEOMAGNETIC FIELD

As discussed in the previous paper (Amenomori et al. 1993a), the Moon’s shadow provides a good estimate of the angular resolution and systematic pointing accuracy of the air shower array at high energies. The angular resolution of this array has been confirmed to be better than 1° by observing the Moon’s shadow (Amenomori et al. 1993a), and the mode energy of primary cosmic rays responsible for generating air showers detected by this array is estimated to be about 8 TeV for protons.

It is also noted that the Moon’s shadow and the geomagnetic field, which acts as a convenient momentum analyzer, enables us to calibrate the results obtained by assigning primary energies to all air shower events. Actually, the deflection angle of a proton of energy E by the geomagnetic field is calculated as $\Delta\theta = 1.6^\circ \times (E/1\text{TeV})^{-1}$ and the direction of this field should make the shadow shift to the west.

We first examine a correlation between the deflection angle of the Moon’s shadow and the air shower size using the events observed with the Tibet-II array. For this, we searched for the deficit center of the Moon’s shadow by dividing the events into four size regions of $15 < \sum \rho < 50$, $50 < \sum \rho < 100$, $100 < \sum \rho < 300$ and $300 < \sum \rho$, where $\sum \rho$ is the sum of the number of particles observed in each detector. Using the Monte Carlo simulation, the mean energies of the primary particles generating the events fallen in respective size regions

are estimated to be about 8 TeV, 15 TeV, 35 TeV and 100 TeV, respectively.

Figure 1 shows the event density map of the Moon’s shadow in each size region, obtained using the events with $\sum \rho > 15$ observed during the period from 1995 to 1997. It is seen that the center of the Moon’s shadow is observed in the direction shifted to the west in small shower size region.

The positions of the most deficit center in respective size intervals are estimated to be $0.21^{+0.15}_{-0.18}^{\circ}$ W, $0.18^{+0.19}_{-0.13}^{\circ}$ W, $0.04^{+0.07}_{-0.08}^{\circ}$ W and $0.04^{+0.08}_{-0.06}^{\circ}$ E, respectively. Here, a maximum likelihood method was used by assuming a 2-dimensional Gaussian type probability function for the event density.

Figure 2 (a) and (b) show the plots between the deflection angle and the mean primary energy in the east-west direction and north-south direction, respectively. As shown in Figure 2 (a), the east-westward displacement of the Moon’s shadow is consistent with that expected from the effect of geomagnetic field, while Figure 2 (b) provides an estimate of the pointing accuracy of the air shower array, which is smaller than 0.1° .

4. YEARLY VARIATION OF THE SUN’S SHADOW

Table 1 shows a yearly variation of the magnitude of solar and interplanetary magnetic fields taken from the data of Stanford Mean Solar Magnetic Field (NOAA/NGDC) and IMP8 (NASA/NSSDC). This table tells us that the strength of IMF near the Earth is rather stable despite changes of solar activity, but the mean strength of solar magnetic field reached a maximum around 1991 and then decreased rapidly with decreasing of the solar activity. This data also shows that the cycle of solar activity reached near minimum between 1996 and 1997.

Shown in Figure 3 is a yearly variation of the Sun’s shadow observed with the Tibet-I and Tibet-II arrays. The observation period for each shadow is as follows : 1991 (1991.4-1991.8) ; 1992 (1992.3 - 1992.7) ; 1996 (1996.3-1996.8) and 1997 (1997.3-1997.8). As discussed in detail in the previous paper (Amenomori et al. 1996), a considerable change is observed between 1990 and 1993 corresponding to the period near maximum or at declining phase of solar activity, and its movement seems to become quick steps after that. It is observed that during the active phase the Sun’s magnetic dipole changed its direction often and abruptly and finally its field polarity was completely reversed. A sudden change of the Sun’s polar fields that caused an asymmetry of the away and toward sector field would create such a large displacement of the shadow in 1991-1993. Therefore, the Sun’s shadow correlates strongly with a variation of large scale structure of the solar magnetic

field changing with the phase of solar cycle.

Compared with the data in 1991 and 1992, however, the Sun’s shadows observed in 1996 and 1997 were found almost at the apparent solar position. In the following we discuss the behavior of the Sun’s shadow observed in the quiet phase of solar activity.

5. SUN’S SHADOW NEAR SOLAR MINIMUM

In Figure 4, we show the event density maps of the Sun’s shadow in four different size regions, which were observed with the Tibet-II array in 1996. Each size interval is the same as that in Figure 1. The observed displacement of each Sun’s shadow in this figure is a superposition of the effects of the solar magnetic field and the geomagnetic field. It is of a great interest to note that the shadow of each size region was observed almost in the apparent direction of the Sun, independent upon the air shower size or primary energy. This suggests that the effects of the solar magnetic field and the geomagnetic field may be canceled each other, resulting in that the shadow remained just in the Sun’s direction. In order to see this in detail, we examined separately an energy dependence of the displacement of the shadow in the away and toward sectors. For this, the Tibet-II data set was divided into three subsets according to the away field (field strength > 0.5 nT), toward field (< -0.5 nT) and boundary field (between -0.5 nT and 0.5 nT) using the IMP8 data (NASA/NSSDC). The fraction of each data set is 3.8 : 3.3 : 2.9.

The displacement of the shadow in the east-west direction is shown in Figure 5(a) for both the away and toward sectors. No obvious displacement is seen for the shadow in each sector, independent upon the primary energy. For the north-southward displacement, however, the Sun’s shadow in each sector of the IMF is shifted in the opposite direction according to the direction of the sector field, and its displacement is symmetric to the ecliptic plane, as seen in Figure 5(b). The Sun’s shadow was not clearly observed in the boundary field because of non-uniformity of the field direction.

It is known that near solar minimum the solar magnetic field is symmetric between the north and south hemisphere of the Sun and the neutral sheet is laid on the ecliptic plane with relatively small warp. The IMF near the Earth is almost parallel to the ecliptic plane and has an Archimedian spiral configuration (Parker 1963). The azimuthal component of this Parker field becomes dominant at large distance from the Sun. Typical crossing angle of this field and Earth’s orbit is about 45° . The field strength decreases inverse proportion to the distance. Average value of this field observed by IMP8 during the period from 1996 to 1997 is 3.4 nT near the orbit of the Earth. The field component at right angles to the

cosmic ray trajectories will make the shadow shift to the north in the away sector and to the south in the toward sector. Furthermore, the geomagnetic field shifts the Sun’s shadow to the west only, since the direction of the Earth’s magnetic dipole is almost parallel to the rotation axis of the Earth. Therefore, the north-southward displacement of the shadow observed in the away and toward sectors can be mostly attributed to the effect of the IMF.

On the other hand, the IMF will scarcely make the Sun’s shadow shift to the east-westward because of a symmetric distribution of the away and toward field to the ecliptic plane in the period near solar minimum. Therefore, the displacement in the east-west direction is, for the most part, caused by the effects of the solar dipole field and the geomagnetic field. The observed results shown in Figure 5(a) suggest that the eastward displacement of the shadow by the solar dipole field was seemingly pushed back by the westward displacement due to the geomagnetic field so that no displacement in the east-west direction was found for the Sun’s shadows observed in the away and toward sectors.

The behavior of the shadow observed in 1997 is almost same as in 1996. We expect that the Sun’s shadow in each sector should show a different behavior according to the change of solar activity as in 1991-1993, and this may be further checked with better statistics during the present solar cycle 23.

6. COMPARISON WITH A SIMULATION

A calculation of the shadows of the Sun and the Moon was made using a simple model of the solar and interplanetary magnetic field (Suga et al. 1999). The assumptions made on the magnetic fields are as follows,

1. For the geomagnetic field, a dipole field with the magnetic moment of $M_E = 8.1 \times 10^{15} \text{ T}\cdot\text{m}^3$ is assumed. The axis of the dipole is inclined at 11.7 degrees from the rotation axis of the Earth.
2. For the solar magnetic field, a dipole field with the magnetic moment of $M_S = B_0 R_\odot^3 = 1.7 \times 10^{22} \text{ T}\cdot\text{m}^3$ is assumed within a radius of about $10 R_\odot$, where B_0 is the field strength at the surface of the Sun and R_\odot the solar radius. The dipole axis is parallel or anti-parallel to the rotation axis of the Sun, that is, perpendicular to the plane of the ecliptic. The field strength of the dipole field at the radial distance r from the Sun’s center is expressed as $B = B_0 (R_\odot/r)^3 \sqrt{1 + 3 \sin^2 \Phi}$, where Φ is the angle measured from the plane of ecliptic. The strength of the dipole field decreases in proportion to r^{-3} and the magnetic moment gives the field strength of $100 \mu\text{T}$ at

the polar surface ($\Phi = 90^\circ$) and $50 \mu\text{T}$ at the equatorial surface of the Sun ($\Phi = 0^\circ$), respectively.

3. The IMF is continuously generated by the steady solar wind blowing from the corona with a constant velocity of $v_r = 450 \text{ km/s}$. The solar wind spreads two-dimensionally in the plane of the ecliptic and the IMF has an Archimedean spiral configuration as the Sun rotates. The radial and azimuthal components of the IMF at the distance r from the Sun are expressed as $B_r = B_0(R_\odot/r)^2$ and $B_\phi \simeq -B_0(R_\odot/r)^2(r\omega_0/v_r)$ ($r \gg R_\odot$) near the equatorial plane, respectively, where ω_0 is the rotation angular velocity of the Sun. Then, $B = \sqrt{B_r^2 + B_\phi^2} \simeq B_0(R_\odot/r)^2 \sqrt{1 + r^2\omega_0^2/v_r^2}$. It is seen that the field strength decreases inversely proportional to r when the distance r is very far from the Sun. Here, the magnitude of B_ϕ is taken to be 2 nT at the Earth's orbit ($r = 1 \text{ AU}$) with the garden hose angle of 45° . The magnitudes of solar dipole field and IMF take the same value of 40 nT at $r \simeq 10.8R_\odot \equiv 0.05 \text{ AU}$, at which the magnetic field is switched from the solar dipole one to the IMF, though the direction of line of force makes a jump. But, this jump has no effect on the result.
4. The IMF near solar minimum consists of four sectors, two away and two toward sectors. Actually the observation data of the IMF (NOAA/NGDC ; NASA/NSSDC) show a structure close to four sectors in the period from 1996 through 1997. These are axial symmetric on the plane of the ecliptic and make the Archimedean spirals. The IMF changes its strength periodically across the sectors in the azimuthal direction. We further assumed that its variation can be described in terms of the sin of azimuth angle for a fixed distance r . The field strength becomes zero on the spiral boundaries between the away and toward sectors and its absolute value reaches the maximum at the center of each sector for the fixed distance r . The root mean square value of the field strength averaging over the azimuth angle is taken to be equal to the value discussed above.

Of course, the solar magnetic field near the Sun is more complicated than the dipole as found by *Ulysses*. It is, however, known that the polarity of the field is opposite in the north and south across the neutral sheet, which is almost parallel to the plane of ecliptic near solar minimum. In this sense, the global field structure near the Sun is similar to that of a dipole, while the high-latitude magnetic field may deviate from the expected dipole geometry according to the *Ulysses* observation (Simth & Balogh 1995 ; Balogh et al. 1995). Also, the Sun's shadow near solar minimum is not so sensitive to the field components in the polar direction. Hence, our model for the solar magnetic field may be a good enough approximation for the present work. Furthermore, such simplification is very helpful in

understanding how the Sun’s shadow is affected by the dipole component of the solar magnetic field.

Trajectories of charged particles are calculated by emitting anti-charged particles from Yangbajing in the wide angular range of $25^\circ \times 25^\circ$ in real angle around the Moon and the Sun. The simulation results were re-sampled by taking into account the energy spectra of primary particles and the angular resolution of the Tibet-II array. Primary particles are assumed to be composed of protons and helium nuclei with a power-law spectrum of $E^{-\gamma}$, where $\gamma = 2.7$ for both particles, since other nuclei give a minor contribution. The flux ratio of protons to helium nuclei is taken to be 1.5. Trigger efficiencies of the events induced by primary cosmic rays were calculated by the simulation.

Figure 6 shows the shadows of the Moon and the Sun obtained by the simulation under the same observation conditions as the experiment. The Moon’s shadow shown in Figure 6(a) is consistent with the experiment, which is shifted to the west by about 0.15° . For the Sun’s shadow, we examined two cases that the dipole directions of the Sun and the Earth are (1) parallel and (2) anti-parallel, respectively. In case of (1) the displacement by the Sun’s dipole is the same direction as that by the Earth’s dipole, while in case of (2) the direction of each displacement becomes opposite. The simulation results by both cases are shown in Figure 6(b) and (c), respectively. The case (2) may correspond to the shadow observed during the period from 1996 to 1997, and it is consistent with the experiment. This simulation may suggest that the most suitable value, M_s , for the magnitude of the Sun’s magnetic moment can be estimated from a detailed analysis of the Sun’s shadow near solar minimum.

We also examined the displacement of the Sun’s shadow by the IMF. The simulation results (Suga et al. 1999) show that the shadow is shifted to the north by the away IMF and to the south by the toward IMF, which are consistent with the experiment as shown in Figure 5(b). Because of a difficulty of separating the away and toward field from the observation data, the observed displacements of the shadow in each sector are slightly smaller than the simulation results. It may be also seen that the Sun’s shadow shown in Figure 4 shows an oval in shape with the major axis in the north-south direction. This deformation can be explained by the effect of IMF.

A comparison with the simulation and the experiment may strongly support the following : 1) Near solar minimum, the displacement of the Sun’s shadow in the east-west direction is mostly caused by the effect of the dipole component of the solar magnetic field ; and 2) the displacement in the north-south direction is due to the effect of the IMF. In the last solar minimum, the effect of the dipole field of the Sun was almost canceled by the geomagnetic field so that the Sun’s shadow seemingly stayed almost in the Sun’s direction.

In the next solar minimum, however, the Sun's shadow will be shifted to the west as in Figure 6 (b) since the polarity of the Sun's dipole is reversed again by that time (case(1)).

7. SUMMARY

Using the data obtained with the Tibet air shower array during the period from 1995 October to 1997 August, we examined the behavior of the Sun's shadow and compared it with a simulation. In this period, the Sun's shadow was observed almost in the apparent Sun's direction, and shows a remarkable difference compared with those observed in 1990 - 1993. It is confirmed that the polarity of the Sun's dipole was reversed in 1992 - 1993 and since then the Sun's dipole has been in the opposite direction to the Earth's dipole (anti-parallel). From a comparison of the observed shadows and the simulation results using a model of the solar and interplanetary magnetic field, we confirmed that the eastward displacement of the shadow due to the solar magnetic field was almost forced back by the effect of the geomagnetic field. We also examined that during this period the IMF made the shadow shift to the north in the toward sectors and to the south in the away sectors. A detailed analysis of the Sun's shadow near solar minimum may enable us to estimate a magnitude of the magnetic moment of the Sun's (equivalent) dipole.

The Sun is now going toward the active phase of the cycle 23 and will reach a maximum around the year of 2001. Then, the angle of the dipole component should rotate from north to south during the cycle, reversing near maximum. The behavior of a dipole may be directly examined from the observation of the Sun's shadow during the period near maximum or at declining phase of solar cycle with a two sector structure of the IMF polarity. During the coming active phase, the Sun's shadow would be found in the direction fairly away from the Sun's direction as in 1990 - 1993, but possibly shifted to the north-eastward, though its direction and magnitude may depend upon the dominance of the dipole component.

A new Tibet air-shower array will be operated in very near future. This array consists of 545 scintillation detectors, which are placed on a 7.5 m grid with a covering area of $2 \times 10^4 \text{ m}^2$. Using this array, air shower events with energy in excess of about 3 TeV can be detected with no serious bias. Then, we can study the Sun's shadow in a wide energy range from 3 TeV to 100 TeV with better statistics. A further observation of the Sun's shadow may provide a unique and important means for clarifying a dynamical change or structure of the solar and interplanetary magnetic fields close to the Sun and also provide new clues how to study the three dimensional configuration of the solar magnetic field under the influence of the solar activity changing with a 11 year period.

This work is supported in part by Grants-in-Aid for Scientific Research and also for International Science Research from the Ministry of Education, Science, Sports and Culture in Japan and for International Science Research from the Committee of the Natural Science Foundation and the Academy of Sciences in China. The authors thank the anonymous referee for critical and valuable comments.

REFERENCES

- Amenomori, M. et al. 1992, Phys. Rev. Lett., 69, 2468
- Amenomori, M. et al. 1993a, Phys. Rev. D, 47, 2675
- Amenomori, M. et al. 1993b, ApJ, 415, L147
- Amenomori, M. et al. 1996, ApJ, 464, 954
- Balogh, A. et al. 1995, Science, 268, 1007.
- Fisk, L.A. 1996, J. Geophys. Res., 101, 15, 547.
- Fisk, L.A. 1997, Proc. 25th Int. Cosmic-Ray Conf. (Durban), 8, 27
- NASA/NSSDC, National Space Science Data Center(NSSDC), *OMNIWeb - Near Earth Heliosphere Data* (URL <http://nssdc.gsfc.nasa.gov/omniweb/>)
- NOAA/NGDC, National Geophysical Data Center(NGDC),
Solar and Upper Atmospheric Data Sources
(ftp://ftp.ngdc.noaa.gov/STP/SOLAR_DATA/SUN_AS_A_STAR/STANFORD/)
- Parker, E.J. 1963, Interplanetary Dynamical Process (New York : Interscience)
- Saito, T. 1975, Sci. Rep. Tohoku Univ., Ser. 5, 23, 37
- Schultz, M. 1973, Astrophys. Space Sci. 24, 371
- Smith, E.J. et al. 1978, J. Geophys. Res. 83, 717.
- Smith, E.J. & Balogh, A. 1995, J. Geophys. Res. Lett., 22, 3317.
- Smith, E.J., Marsden, R.G. and Page, D.E. 1995, Science, 268, 1005.
- Suga, Y. et al. 1999, Proc. 26th Int. Cosmic-Ray Conf. (Salt Lake City), 7, 202
- Svalgaard, L. & Wilcox, J.M. 1978, Ann. Rev. Astron. Astrophys. 16, 429, 1978

Wilcox, J.M. & Ness, N.F. 1965, J. Geophys. Res., 70, 5783

Year	1990	1991	1992	1993	1994	1995	1996	1997	1998
Stanford (μT)	47.0	72.1	34.1	26.4	23.6	14.7	9.1	8.9	17.6
IMP8 (nT)	5.1	6.4	5.7	4.4	4.3	3.7	3.1	3.7	3.7

Table 1: Yearly variation of the mean strength of solar magnetic field and IMF near the Earth.

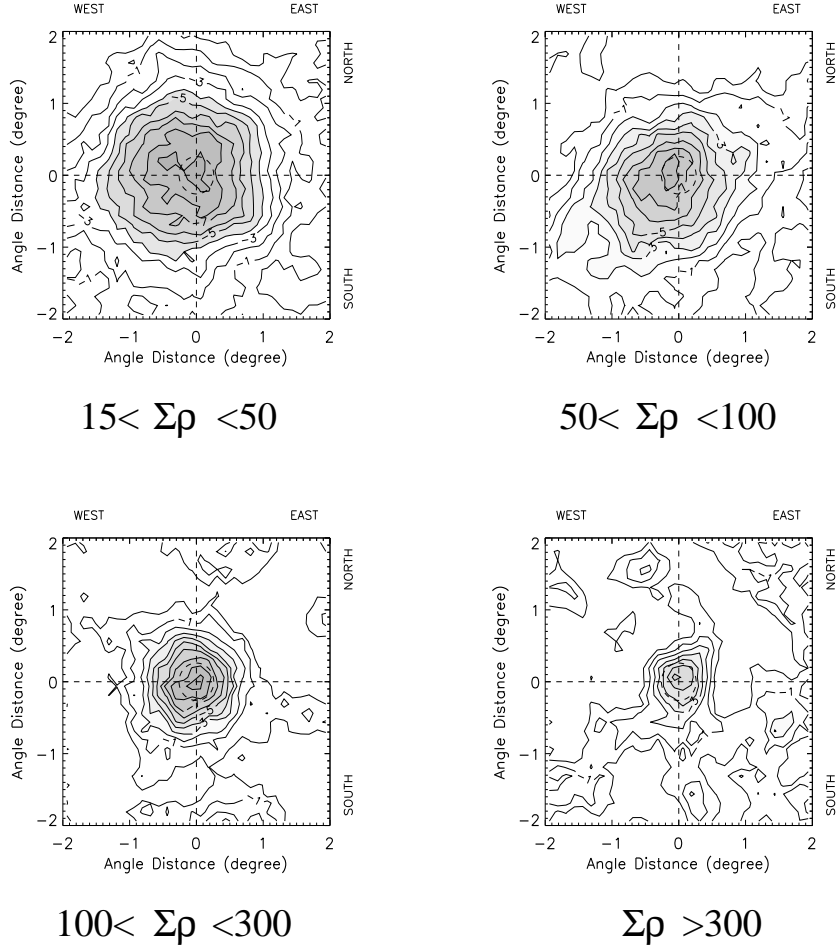


Fig. 1.— Energy dependence of the displacement of the Moon’s shadow. The contour map of each shadow gives the weight of deficit event density from the background, and contour lines start from 0σ deficit with a step of 1σ . Same definition is used in the following figures.

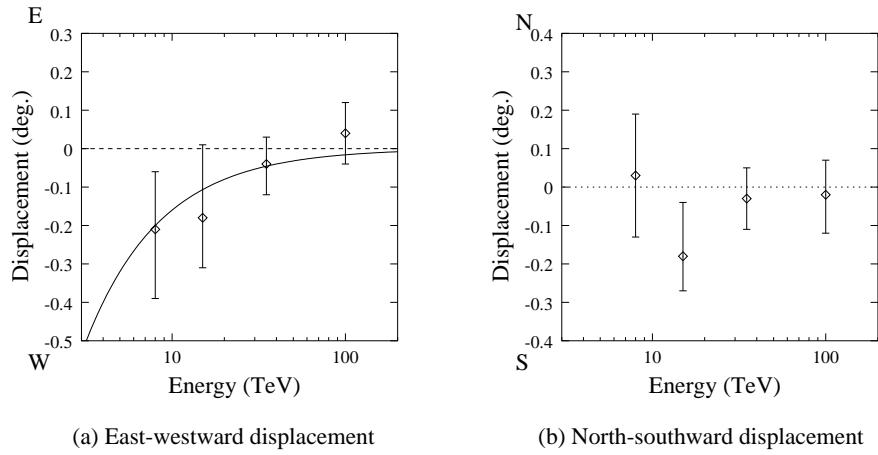


Fig. 2.— Energy dependences of the displacements of the Moon’s shadow in the east-west direction (a) and north-south direction (b), respectively. Solid curve in (a) shows the expected deflection angle of a proton by the geomagnetic field.

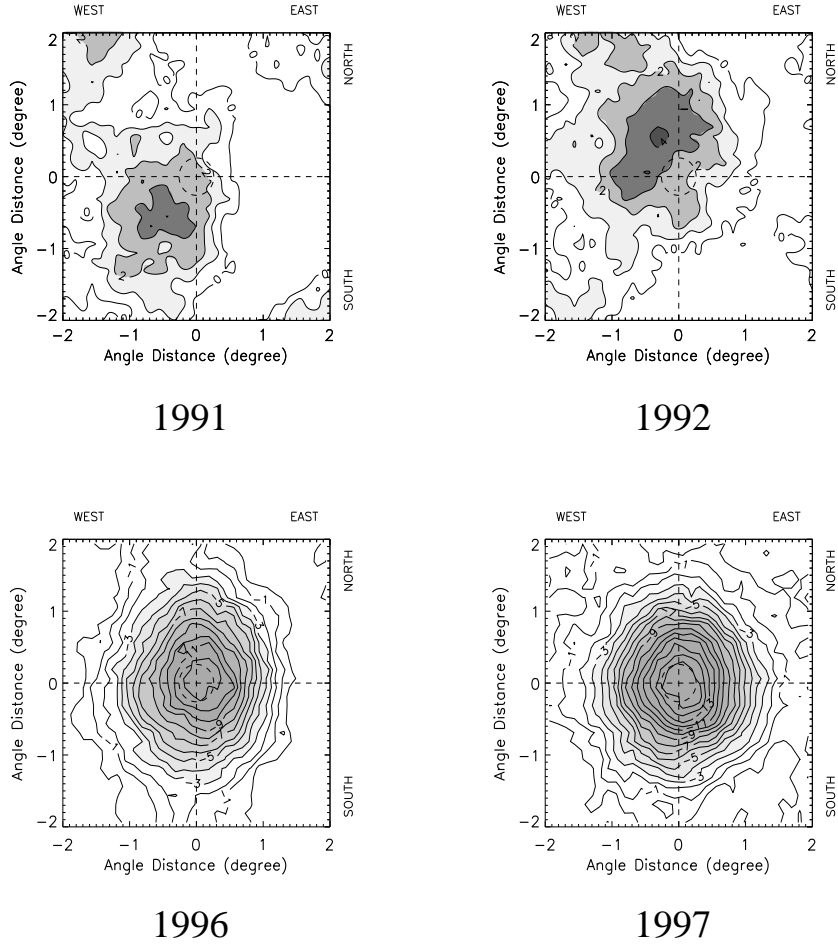
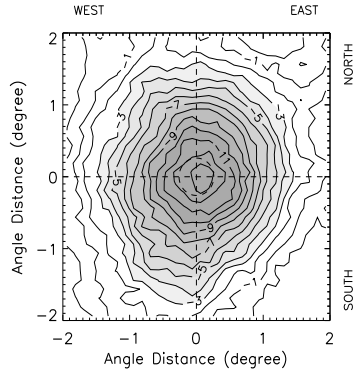
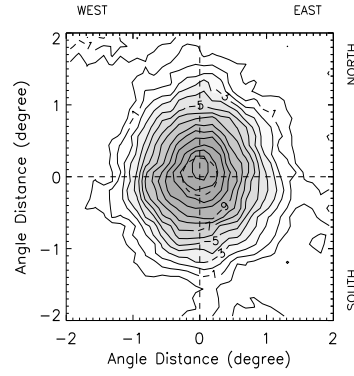


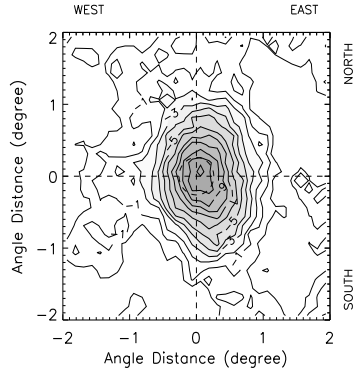
Fig. 3.— Yearly variation of the Sun’s shadow. Each shadow is obtained using all events with $\sum \rho > 15$ and the mode energy of primary protons is estimated to be about 8 TeV.



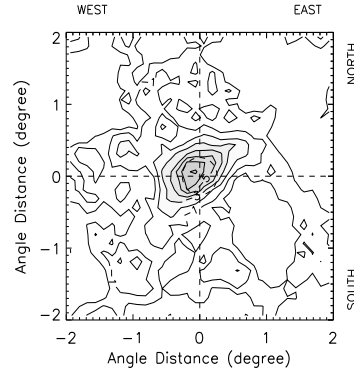
$$15 < \Sigma\rho < 50$$



$$50 < \Sigma\rho < 100$$



$$100 < \Sigma\rho < 300$$



$$\Sigma\rho > 300$$

Fig. 4.— Dependence of the Sun's shadow upon the air shower size, observed in 1996.

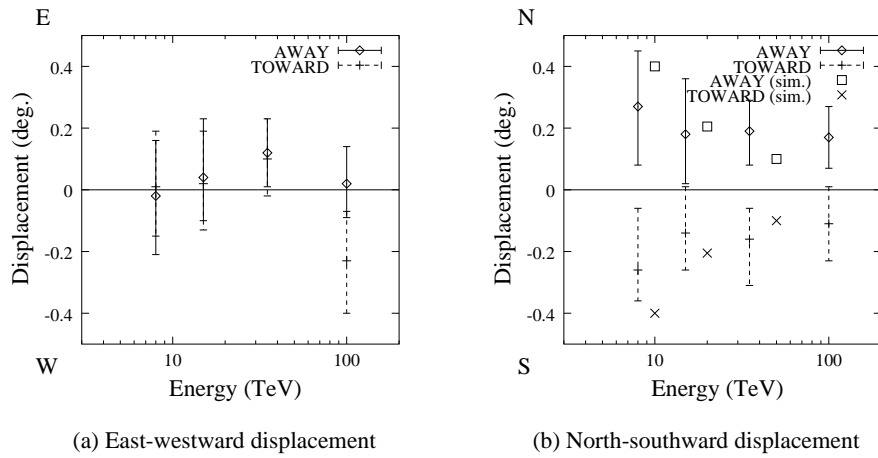


Fig. 5.— Energy dependence of the east-westward (a) and north-southward (b) displacement of the Sun’s shadow. Minus and cross markers denote the displacement of the Sun’s shadow for the away IMF and toward IMF data sets, respectively. The simulation results (squares : away ; crosses : toward) are compared with the experimental data.

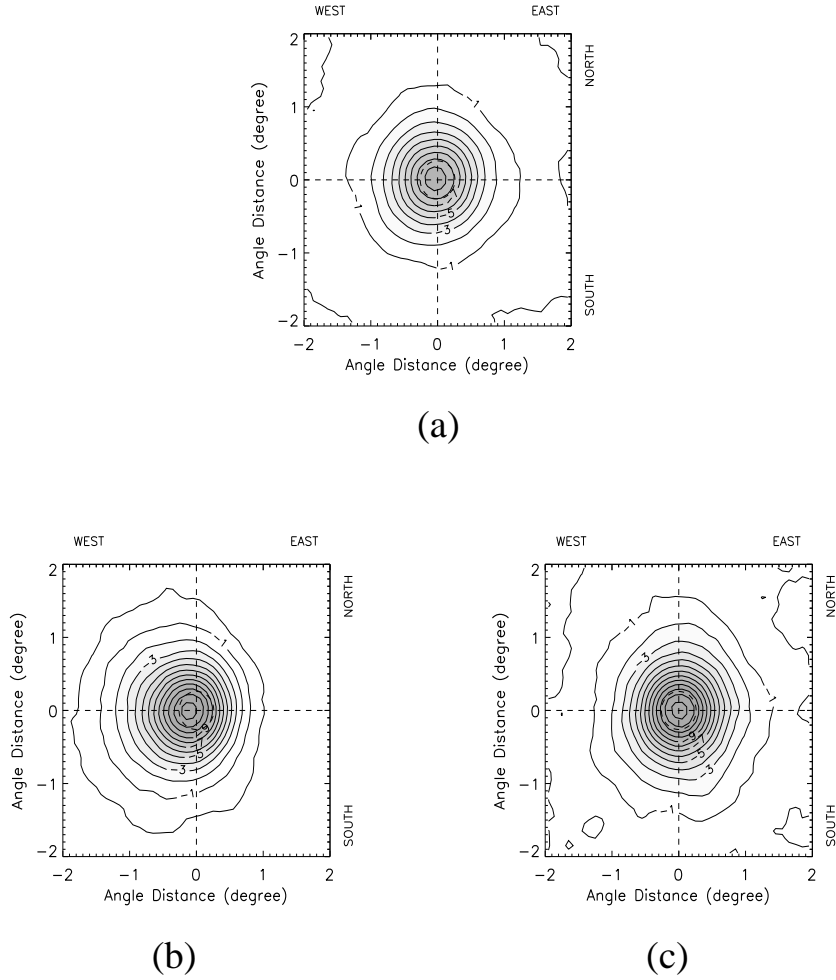


Fig. 6.— Shadows of the Moon and the Sun obtained by the simulation (all events with $\sum \rho > 15$). (a) Moon’s shadow, (b) Sun’s shadow in case of parallel dipoles and (c) Sun’s shadow in case of anti-parallel dipoles.